SANDIA REPORT

SAND2004-6388
Unlimited Release
Printed January 2005

Quantum Squeezed Light for Probing Mitochondrial Membranes and Study of Neuroprotectants

Paul L. Gourley, Robert G. Copeland, Anthony E. McDonald, Judy K. Hendricks, and Robert K. Naviaux

Approved for public release; further dissemination unlimited.

Sandia National Laboratories

Quantum Squeezed Light for Probing Mitochondrial Membranes and Study of Neuroprotectants

Paul L. Gourley, Robert G. Copeland, and Anthony E. McDonald
Biomolecular Materials and Interfaces Department
Sandia National Laboratories
P. O. Box 5800
Albuquerque, NM 87185-1413

Judy K. Hendricks
Contractor

Robert K. Naviaux,
Departments of Medicine and Pediatrics
University of California, San Diego 92103-2071

ABSTRACT

We report a new nanolaser technique for measuring characteristics of human mitochondria. Because mitochondria are so small, it has been difficult to study large populations using standard light microscope or flow cytometry techniques. We recently discovered a nano-optical transduction method for high-speed analysis of submicron organelles that is well suited to mitochondrial studies. This ultrasensitive detection technique uses nano-squeezing of light into photon modes imposed by the ultrasmall organelle dimensions in a semiconductor biocavity laser. In this paper, we use the method to study the lasing spectra of normal and diseased mitochondria. We find that the diseased mitochondria exhibit larger physical diameter and standard deviation. This morphological differences are also revealed in the lasing spectra. The diseased specimens have a larger spectral linewidth than the normal, and have more variability in their statistical distributions.

This page left intentionally blank

Contents

**This page left intentionally blank**

Introduction

Semiconductor Laser Technology for Biomedical Science

Laser technology has advanced dramatically and is an integral part of today's healthcare delivery system. Lasers are used in the laboratory analysis of human blood samples and serve as surgical tools that kill, burn or cut tissue. Recent semiconductor microtechnology has reduced the size of a laser to the size of a biological cell or even a virus particle. By integrating these ultra small lasers with biological systems, it is possible to create micro-electrical mechanical systems (MEMS) that may revolutionize health care delivery. BioMEMS devices are rapidly finding new applications for chemical analysis, molecular detection, and health care [1-5]. One is a biolaser device [6–11] that confines intense light into an extremely small interaction volume. The biolaser has been integrated with a microfluidic chip (shown in figure 1) and recently been applied to assess cell structure. It has shown the ability to probe the human immune system by using optical size effects to measure cell and nucleus dimensions of lymphocytes [9], characterize genetic disorders (quantify sickled and normal red blood cell shapes and hemoglobin content) [7,10,] and distinguish cancerous from normal cells [6,11]. Most importantly, cells can be analyzed immediately after they are removed from the body. There are no time delays or difficulties associated with chemical fixing or tagging cells with stains or fluorescent markers. Semiconductor laser materials like GaAs, AlAs, InP, InGaN can also be applied to photodynamic therapy [12], optical tomography [13], cell micromanipulation [14, 15], and laser cytometry [16–18]. The applications of such a portable biological sensing device are potentially far-reaching. One envisioned surgical application is a 'smart scalpel', for online flow cytometry in the operating room. It would provide a form of real-time biopsy that would give surgeons and their patients confidence that all of the diseased tissue had been removed during surgery [6].

Structure and Operation of the Biological Microcavity Laser

A typical laser used in biophotonics applications is used to irradiate external cells or tissues, e.g. for diagnosis by cytometry and fluorescence imaging and spectroscopy [19, 20]. In contrast, the biocavity laser uses a cavity formed between a semiconductor light-emitting material and an external dielectric mirror surface to enclose a single cell (flowing or stationary), which acts as an internal waveguide as shown in figure 1. The sample may be whole blood, cells from culture, tissue from a biopsy or a scraping of body tissue (such as that obtained during a cervical cancer test). Most specimens, when placed into the biocavity laser behave like tiny lenses as light traverses the specimen near 850 nm. Human tissue and cells have low absorption between 600 and 1200 nm, the so-called therapeutic zone for laser treatment. Because the cells are very transmissive at these wavelengths, they are sampled hundreds of times as the light bounces between the mirrors.

In the present work, the laser wavelength is centered in the low absorption zone, near 830 to 840 nm. With only fluid in the cavity (left-hand side of figure 1), stimulated emission is observed only for a single light frequency (blue rays) that appears as a single peak in output spectrum. With a cell present (right-hand side of figure 1), the speed of light is slowed and multiple light paths are available through the cytoplasm (green rays) and nucleus (red rays). The waveguiding of the rays reflected back through the cell establishes an image of the transverse cell modes in the semiconductor gain region. Because the refractive index of the cell is higher than that of the bare fluid, the spectrum is red-shifted and comprises a series of spectral peaks from the cytoplasmic and nuclear modes. The peak spacing, intensity and red-shift are sensitively dependent upon the cell size, shape and biochemistry, respectively, as shown in previous analyses [6].
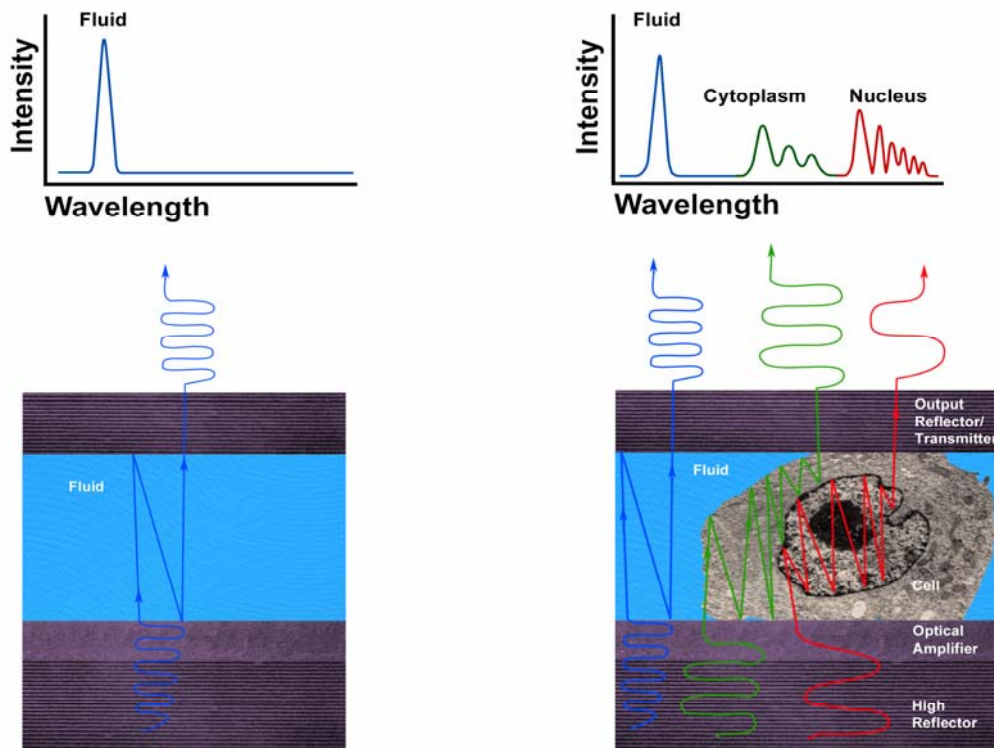
Fig. 1. Schematic of biocavity laser with fluid only (lower left) and emitted spectrum (upper left). Right side shows the biocavity with cell and corresponding spectrum. medium.

The biocavity can be used to measure the concentration of biomolecules in a solution or in a living cell using refractive spectroscopy [6]. When a fluid is flown into the cavity, the resonant peaks in the spectra will shift according to the refractive index of the solution. There is a linear relationship between the refractive index and the biomolecular concentration as $n = n_0 + \alpha C$ where n_0 is the water index, α is the specific refractive increment of the molecule, and C the concentration in grams per 100 ml. By calibrating the spectral shift induced by solutions of known protein concentration and refractive index, an unknown protein concentration can be determined.

Application of the Biocavity Laser to Study Mitochondria

Mitochondria in the Biocavity Laser and Nano-squeezed Light

Because the mitochondria are so tiny, it has been difficult to study them using standard light microscope or flow cytometry techniques. And, electron or atomic force microscopies are limited to nonviable, fixed organelles so they cannot reproduce physiologic measurements. We have recently discovered a nano-optical transduction method for high-speed sensing of submicron organelles like mitochondria [21,22]. This ultrasensitive detection of submicron particles uses quantum squeezing of light into photon modes imposed by ultrasmall dimensions in a submicron laser cavity. It has the potential to rapidly probe the morphology and biochemistry of the organelle in a near-physiologic state.

We have studied lasing spectra for a variety of bioparticles ranging over 2 orders of magnitude in size from 30 microns to 300 nm. The laser light is spatially/temporally resolved, recorded by digital video imaging, and analyzed with fast spectral recognition algorithms. These laser hyperspectra are sensitive to scattering from the distribution of protein molecules in organelles and cells. As the diameter decreases, the number of quantized photon modes decreases from about 100 to 1 as the particle approaches submicron dimensions. In this regime where the particle is smaller than the wavelength of light, nano-squeezing of light and inhibited spontaneous emission influences the emitted spectra. These quantum optic effects enhance the detection sensitivity of submicron particles. Under conditions of small number of photon modes, the lasing efficiency is increased significantly. Such dramatic increases in light signals allows an entirely new method of optical transduction.

Light Scattering from Cells and Organelles

To understand how mitochondria will influence the laser spectra, it is helpful to consider how light interacts with organelles and cells. These interactions are summarized in Fig. 2 by showing the biological particle on the left side and the corresponding light scattering distributions (parallel and perpendicular to plane of incidence) on the right side. Many cell organelles and tubules of endoplasmic reticulum and protein molecules are smaller than the wavelength of visible light. Light scattering by such small particles is known as Rayleigh scattering and the particle behaves as a dipole and radiates in all directions.

By far, the largest contribution to scattering in cells is due to Mie scattering from such as mitochondria. These organelles occur in larger numbers ($\sim 10^{12}$ cm^{-3}) and of appropriate size near the wavelength of light (~ 500 nm) to make this one of the dominant scattering effects. Mie scattering and can include scattering from large organelles, the nucleus, and the cell as a whole. The nucleus and cell are relatively large and have index differences of a few percent compared to the fluid and cytoplasm, respectively. Light is scattered at small angles by larger objects with slight differences in refractive index relative to the surrounding fluid.

The cell is significantly larger than the wavelength of light and produces a more forward geometrical scattering patterns as shown in the top of Fig. 2. The approximate theory of light scattering by large spherical particles was first proposed by Van de Hulst [23] and can be extended to large particles of an arbitrary shape. Early and later studies of light scattering by cells [23-29] found good agreement with Mie theory when the cell was approximated as denser sphere imbedded into a larger and softer sphere. The sizes of the spheres corresponded to the average sizes of the cell nuclei and cell, respectively. This agreement existed despite non-homogeneity and non-spherical shape. Particles large compared to the

wavelength produce the scattered field that peaks in the forward and near backward directions in contrast to smaller particles, which scatter light more uniformly. The angular width of the forward peak, is proportional to the ratio of the wavelength λ to the particle's size a as $\theta = \lambda/a$.

OPTICAL SCATTERING IN CELL COMPONENTS
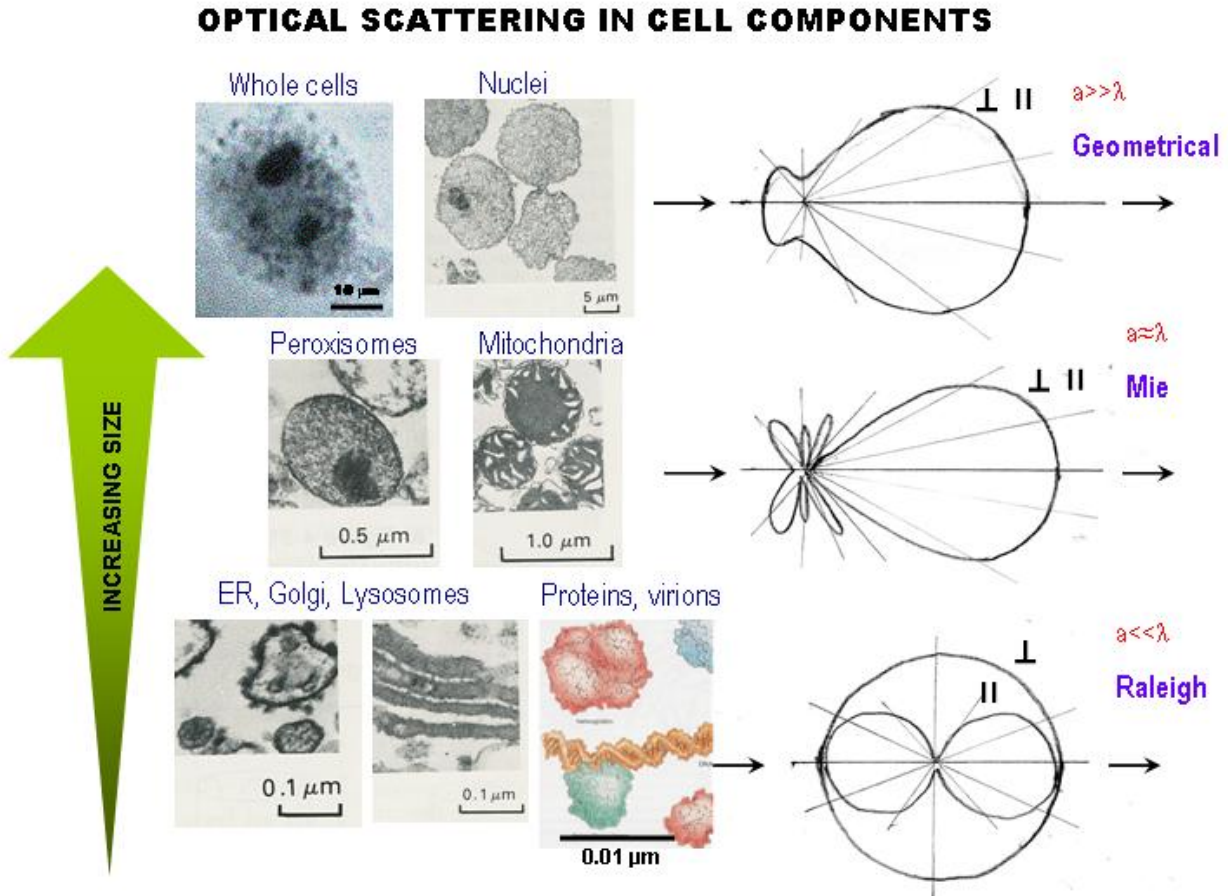
Fig. 2. Images of cell components of various sizes (left side) and corresponding light scattering intensities distributions for light parallel and perpendicular to the plane of incidence (right side).

Effect of Light Scattering on Lasing in the Microcavity

Light scattered at small angles is reflected multiple times in the cavity and builds up stable lasing modes in the lasing process. The large angle scatter light is lost sideways from the longitudinal cavity. The Rayleigh mechanism tends to scatter light at large angles relative to the incident beam. Thus, these tend to be loss mechanisms for operation of the laser which operates principally with light in the forward and backward directions. The reflected light cycles through the cell, cavity, and semiconductor gain region till a stable mode pattern is formed. Cells or organelles inside the microcavity also serve as optical waveguides to confine light generated in the resonator by the semiconductor. The waveguiding effect is due to slight differences in the dielectric constants between various cell components and the surrounding fluids. The laser operates at resonant frequencies established by the dielectric properties of the cells. By using a high resolution spectrometer, these lasing frequencies can be resolved into narrow spectral peaks. The spacing and intensity distribution between peaks provides a unique spectral signature for each

different cell as shown in Fig. 3 for a small bacterial cell (upper spectrum) and a large cell (lower spectrum). Interpretation of these spectra can be guided by analytical solutions of the Helmholtz wave equation for an optical microcavity.
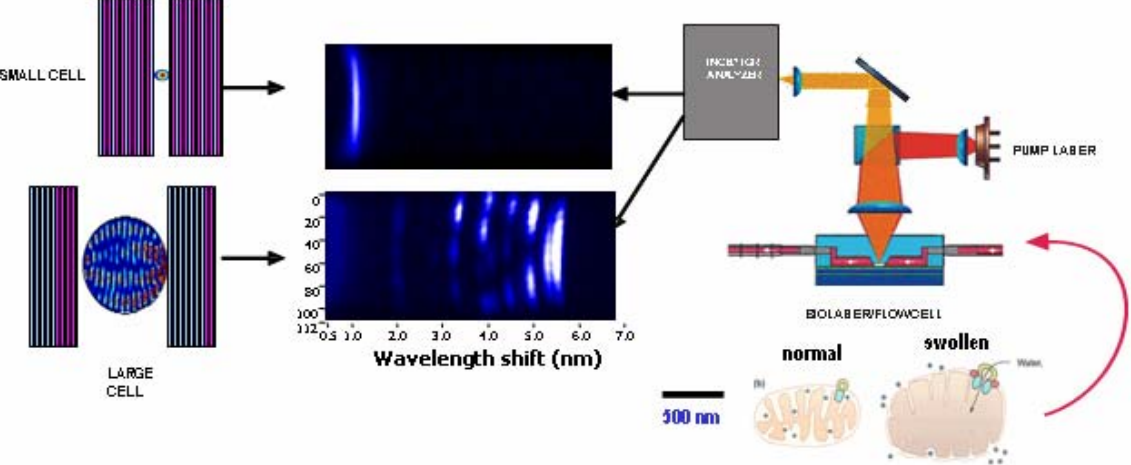
Fig. 3. Right side: experimental arrangement to measure lasing spectra of mitochondria. Middle images show spectra for small (top) and large cell (bottom).

Previous Experiments with Mitochondria in the Biolaser

Ca^{+2} Induced Swelling of Mitochondria

Mitochondria exist in virtually all eucaryotic cells and are essential to the normal life of animal cells as the main producers of ATP through aerobic respiration. During the last decade, mitochondria have been increasingly implicated in playing an active role in the life/death decisions of the cell. The inner mitochondrial membrane is normally impermeable to solutes not endowed with specific transport systems. As a result of Ca^{++} accumulation, oxidative stress or in vitro aging, mitochondria may undergo a sudden permeability increase of the inner membrane to solutes of molecular mass up to 1500 Da. This phenomenon is described as the mitochondrial permeability transition (mPT) or permeability transition pore (PTP). Pathophysiologic mPT is observed to constitute a critical event in apoptotic as well as necrotic cell death [30-45].

We have recently reported nanolaser measurements of Ca^{+2} induced swelling of the inner membrane, with attendant creation of megapores and release of toxic cytochrome c into the cytoplasma [21,22]. Such swelling effects has been implicated in Parkinson's, Huntingtons, Alzheimer's diseases, and amyotrophic lateral sclerosis. It is also implicated in the harmful effects on the central nervous system of soldiers exposed to radiation or nerve agents. Efforts to find neuroprotectant drugs to avoid mitochondrial membrane dysfunction and swelling have become important for both healthcare and national defense.

The experimental apparatus to study mitochondria is illustrated in Fig. 3. Liver cells were harvested from mice, lyzed, and centrifuged to separate the mitochondria. The mitochondria were then suspended in a solution of HEPES buffer in preparation for flow experiments. Typical concentrations were in the range of 100,000 organelles per ml of solution. This solution was used as the control. In addition, a separate solution of CaCl ranging from 10 to 1000 μM was added to produce an insult to the organelle and induce swelling. The organelles were flowed for a few minutes and the emitted spectra were recorded and analyzed to extract spectral parameters such as spectral wavelength, linewidth, intensity and others.

The changes in the spectral parameters are summarized in Fig.4 which plots the wavelength shift (solid points) and linewidth (open points) as a function of Ca^{++} concentration. The standard deviations are represented by the error bars which surround each point. These data show measurements of mitochondria spectra under normal conditions and under high calcium ion gradient conditions that upset membrane homeostasis and lead to organelle swelling and lysis, similar to that observed in the diseased state. The measured spectra are consistent with calculations of the electromagnetic modes in normal and distended mitochondria using multiphysics finite element methods described below.
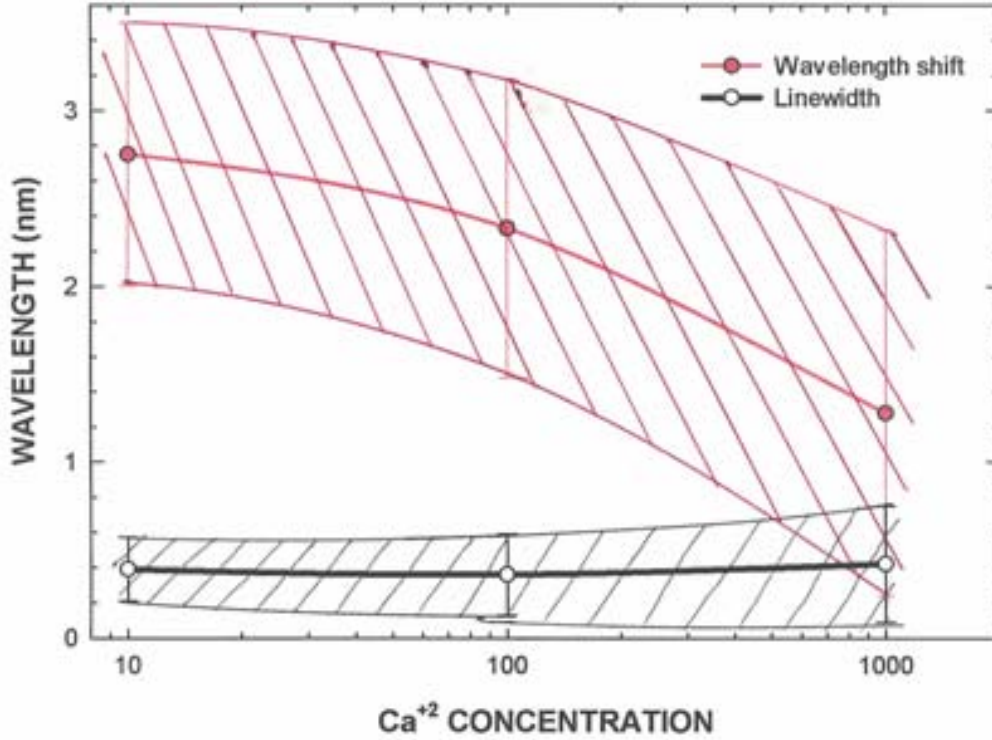
Fig. 4. Summary of spectral data for Ca^{++} insulted mitochondria. The solid points are the mean wavelength shift and the open points are the mean spectral linewidth. The error bars surrounding each point represent the standard deviation measured for both parameters

Laser Frequency Analysis

In addition to the experiments, have developed numerical models of mitochondria photonics and membrane swelling using multiphysics finite element codes. Initially, we investigated numerical solutions to the electric field distribution and modal frequencies for spheroids in a cavity, to approximate mitochondria. Parametric studies were carried out to determine the eigenfrenquency dependence on sphere radius r and refractive index $\Delta n = n_2 - n_1$, the difference between the spheroid n_2 and the surrounding fluid index n_1 (taken as water). The relative change in the fundamental eigenfrequency $\delta = -(\omega-\omega_0)/\omega_0$, where ω_0 is the cutoff frequency was determined as the empirical relationship

$$\delta(r, \Delta n) \approx 0.0232\Delta n \, r^{2.7} \tag{1}$$

where r is in microns. Thus, the relative frequency change is nearly proportional to the optical volume $4\pi\Delta n r^3/3$. Since mitochondria vary in shape from spherical to prolate spheroids, to ellipsoidal, the calculation was repeated for ellipsoidal shapes with major and minor axes in the ratio of 2 to 1. The dependence of frequency on major axis dimension was similar to the case for spheres.

Study of Normal and Diseased Mitochondria in the Biolaser

To further examine biolaser analysis of mitochondria, we examined a set of 7 mitochondrial specimens, including both normal and diseased. The diseases specimens included both cytochrome oxidase genetic deficiencies and specimens from patients.

Microscopic Imaging of Mitochondria

The normal and diseased mitochondria were studied in the reflection mode of a laser confocal microscope at 488 nm to determine their average diameter and standard deviation. Typical images of the mitochondrial specimens are shown in the left side image of Fig. 5. All of the mitochondria from each of the sample suspensions appeared very uniform and circular, having the appearance of Airy disks due to optical diffraction of the reflected light. One specimen (right side of Fig. 5) comprised mitochondrial with additional rod-shaped cells of length 2 μm and width 400 nm of much lower concentration. There are probably bacterial cells that contaminant the specimen, but serve a useful function to compare effects of submicron cell morphology on lasing spectra.
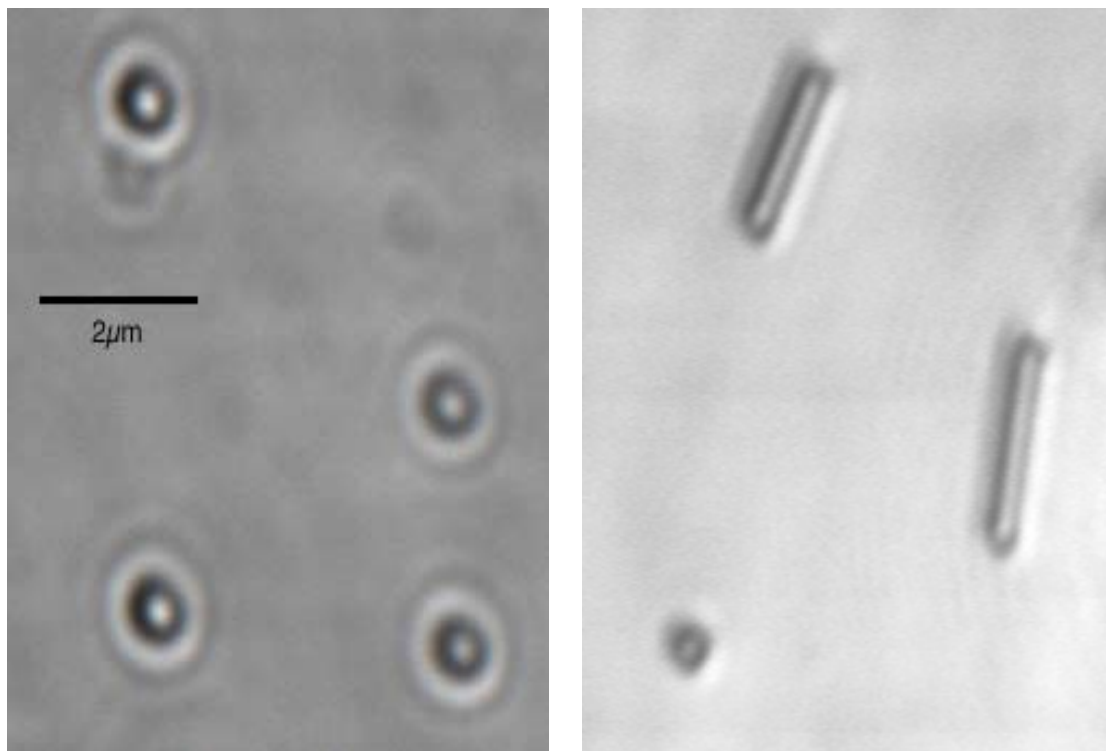
Fig. 5. Laser scanning confocal scanning microscope images of a normal mitochondrial specimen (left side) and diseased specimen SM containing rod-shaped cells (right side).

The diameters of about 50 mitochondria per specimen were measured using a calibrated scalebar. Both the mean and standard deviation of the ensemble of measurements were determined and plotted in Fig. 6.

These data reveal that the average diameter of the normal mitochondria is in the range 680 to 730 nm with standard deviation of about 35 nm. The diseased mitochondria exhibited a larger mean diameter in the range 750 to 830 nm with a much larger standard deviation of about 70 nm. Thus, diseased mitochondria appear about 15% larger than normal mitochondria, and they are about 2 times as variable.
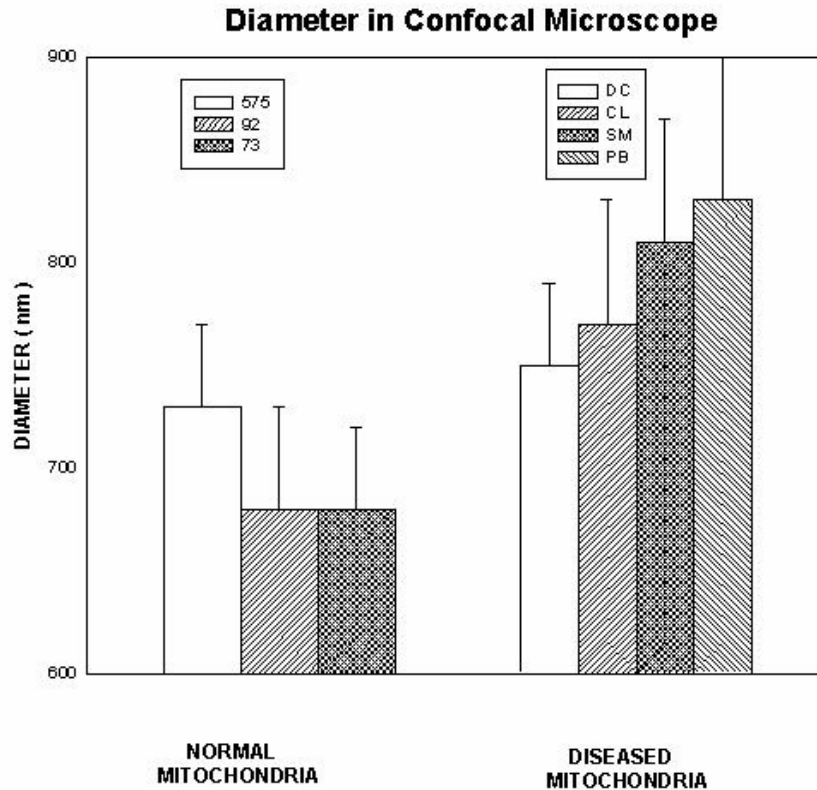
Fig. 6. Average diameter (vertical bars) and standard deviation (vertical lines) for normal and diseased mitochondria.

Biocavity Laser Spectroscopy of Mitochondria

The mitochondria were prepared in suspension and examined with the biolaser using the following procedure. The initially concentrated mitochondria (in range 10^6 to 10^7 organelles/ml) were diluted a factor of 10 in 20 mM HEPES and 6 mM Sorbitol buffer. The mitochondria were then flowed through the biocavity laser with cavity length of a few microns. As the mitochondria flowed through the optical gain region in the microcavity, they triggered lasing action to generate a beam of light. That beam was focused onto an imaging monochromator and detected with an imaging camera. The camera images recorded the spectral and angular distribution of the far field of the lasing beam.

Three representative images of the spectra for 3 different specimens are shown in Fig. 7. In contrast to the more complicated images detected in beams from whole cells (see lower spectra of Fig. 3), the mitochondria lasing images are usually quite simple. Most often they comprise only one or two lasing peaks. This is the case for the spectral images from individual mitochondria from normal and diseased

specimens shown in the top two images of Fig. 7. For these spectra, the spectral position, spectral linewidth, lasing intensity, and angular spread were extracted from the camera image.
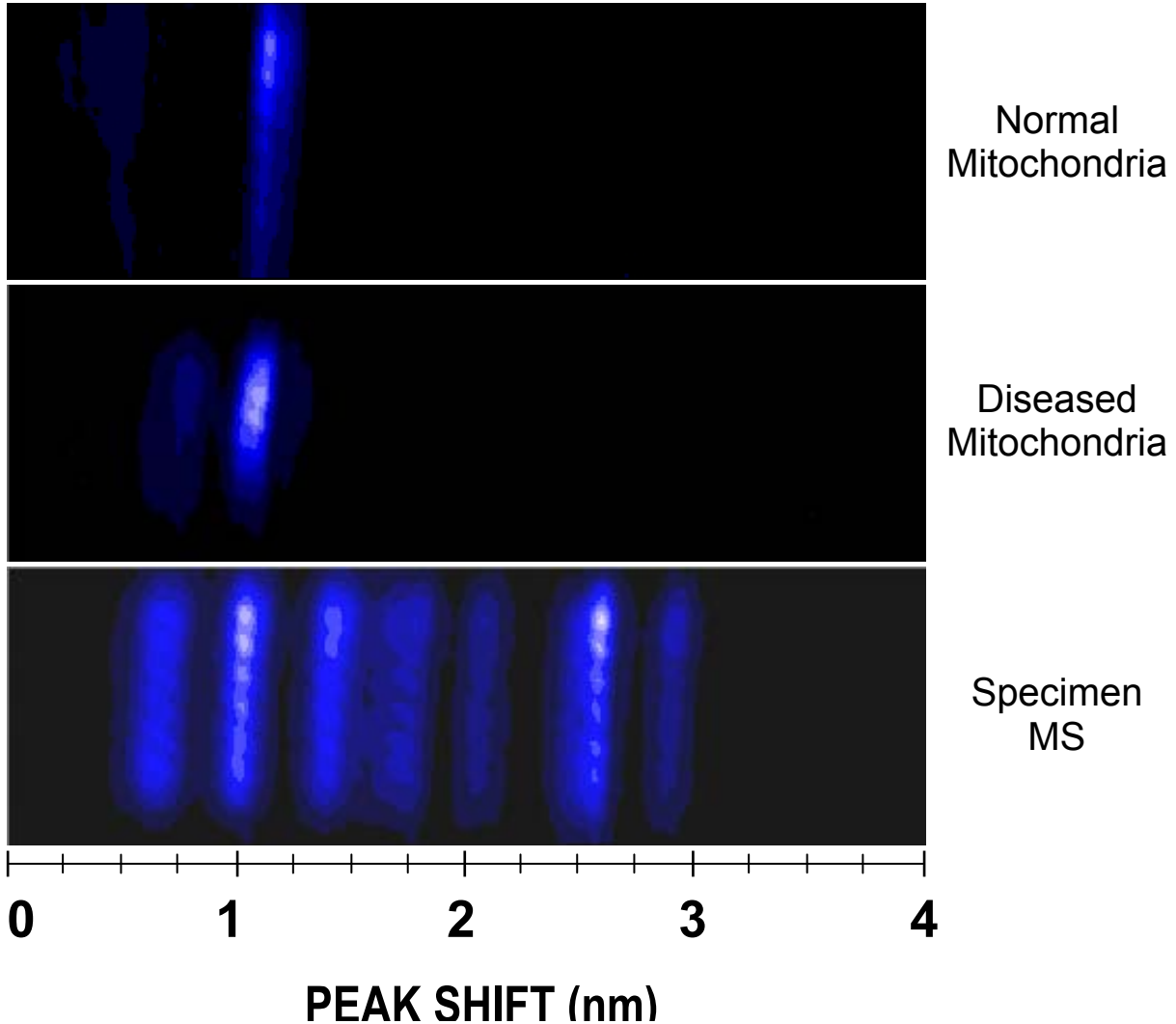
Fig. 7. Typical laser spectral images of normal (top) and diseased (middle) mitochondria. The Lower image is taken for an unusual specimen that exhibits many regularly spaced lines.

The first three parameters were plotted in 3-dimensional cluster plots like those shown in Fig. 8 for normal (upper plot) and diseased (lower plot) mitochondria specimens. The cluster plot for normal mitochondria shows a wavelength shift (peak shift 0 label) mostly near 1 nm and tapering off to 5nm. The smallest wavelength shift is correlated with smallest linewidth and smallest intensity. We expect the smallest mitochondria to produce the smallest wavelength shift because they have the smallest filling factor in the laser cavity. The correlations with the other spectral parameters are less understood, but define a fingerprint that helps to distinguish the normal mitochondria. The plot for the diseased specimen

16

reveals a distinctly different cluster shape than the normal. The wavelength shift is less correlated with the other spectral parameters.
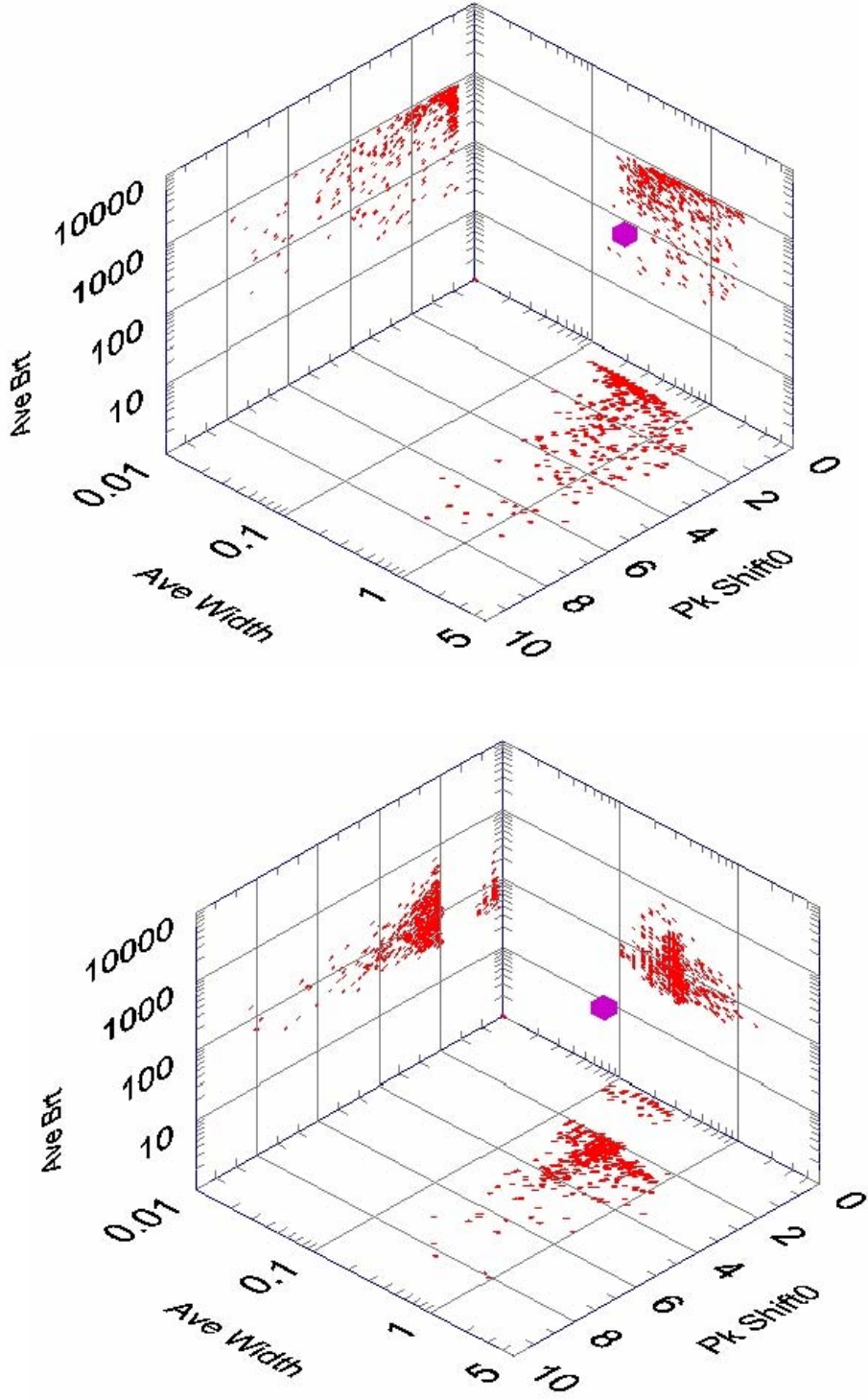
Fig. 8. Cluster plots of normal (upper plot) and diseased (lower plot) mitochondrial specimens.

The mean spectral linewidth and standard deviation of all of the normal and diseased mitochondria specimens are summarized in Fig. 9. The data show that the spectral linewidth is significantly broader for the diseased specimens. The normal linewidth is in the range 0.30 to 0.45 nm, but the linewidth for diseased specimens is 0.40 to 0.85 nm, about 100 to 200% larger. The standard deviation for the normal specimens is 0.20 to 0.40 nm, and 0.30 to 0.60 nm, about 50% larger, for diseased mitochondria.
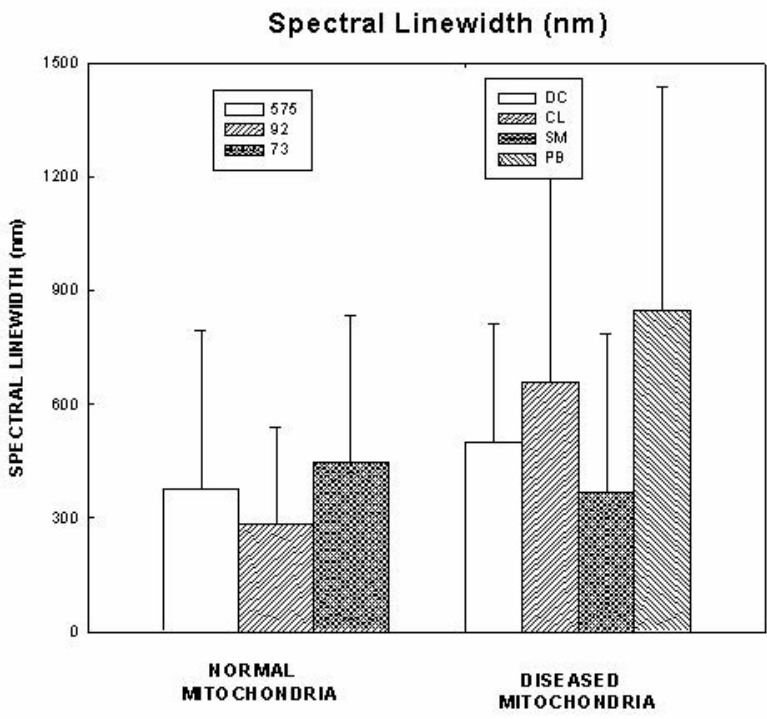
Fig. 9. Average spectral linewidth (vertical bars) and standard deviation (vertical lines) for normal and diseased mitochondria.

Finally, in Fig. 10 we show a cluster plot corresponding to the mitochondrial specimen that comprised a significant number of rod-shaped cells. These were shown in the laser scanning confocal microscope image (right image in Fig. 5) which were probably bacteria. These spectra are dominated by the rod-like cells and reveal an unusual comb-like spectrum of regularly spaced peaks between 1 and 6 nm. Regularly spaced spectral peaks are expected for linear cells like rods and have been previously discussed for the case of sickled red blood cells [10]. These data demonstrate that the spectra are quite sensitive to the morphology of the cell specimens.

18
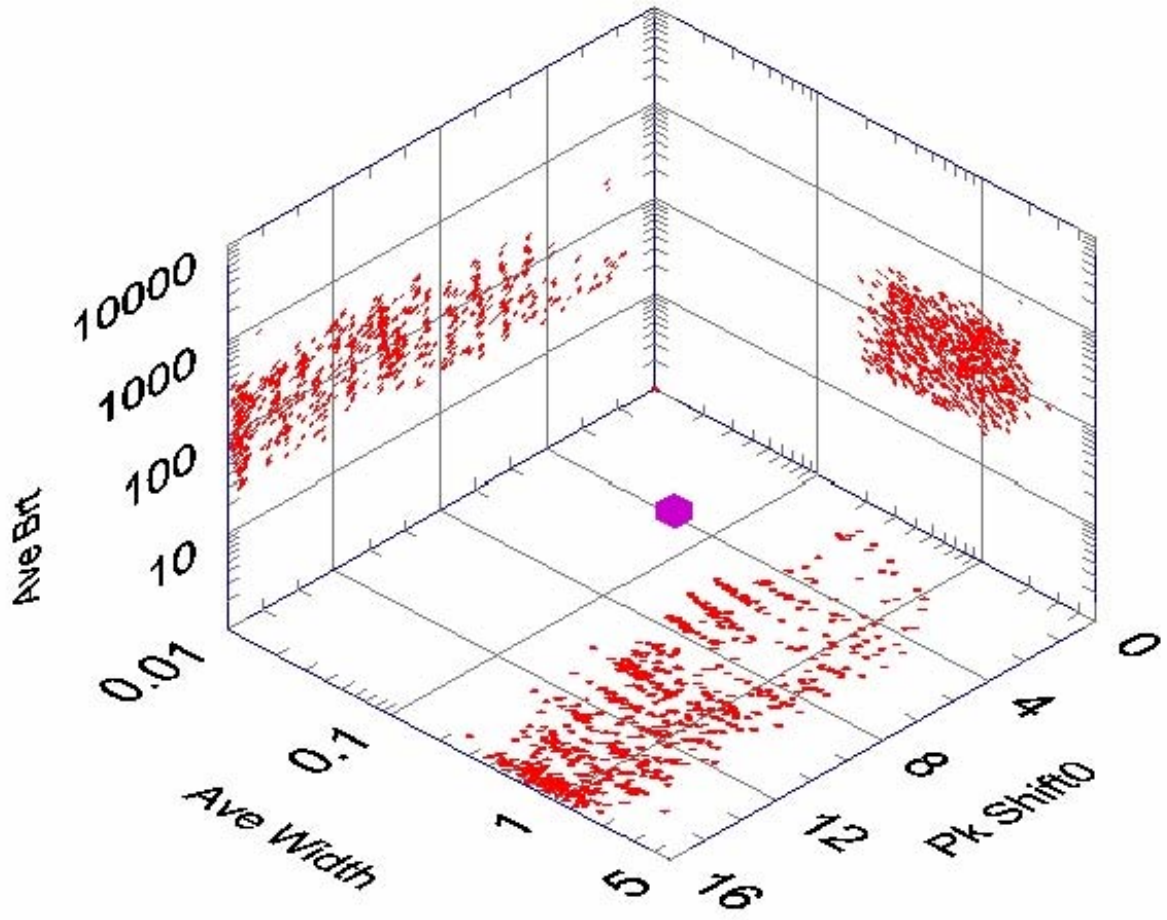
Fig. 10. Clutster plot for specimen SM comprising both mitochondria and rod shaped cells

Discussion and Summary

Mitochondrial organelles are very tiny particles as small as the wavelength of light. Detection and analysis of these ultra-small particles requires new spectral-imaging techniques with high sensitivity. We have presented such a technique using nano-squeezing of spontaneous light emitted through a mitochondria flowing at high speed in a biocompatible semiconductor microcavity. This nano-squeezing allows even tiny organelles to generate a large spectral signal that can be easily detected. The spectral images were rapidly recorded and analyzed in a spectral image analyzer. The laser light is spatially and spectrally analyzed within seconds using efficient image recognition software. The technique was initially applied to mitochondria that had been osmotically swollen by high calcium ion gradients. The method showed that it could rapidly measure the swelling effect. We also applied the technique to normal and diseased mitochondria and showed that the diseased mitochondrial spectra varied significantly from those for normal mitochondria. In addition, we compared mitochondria spectra to spectra from small rod-shaped cells present in one mitochondrial specimen. These data reveal that this technique is sensitive to different particle shapes.

The laser spectral analysis of the mitochondrial specimens was performed with light of near infrared (NIR) light in the range 830 to 850 nm. While living tissue is largely transparent to NIR wavelengths it contains a number of constituents which absorb specific components in this spectrum. Some of these compounds such as hemoglobin and cytochrome oxidase are of particular interest because of their direct connection to metabolic processes. For example, a significant amount of research has been directed at examining the use of NIR spectroscopy to look at the oxidation state of cytochrome oxidase in relation to brain hypoxia [46-48]. The biocavity laser's operation in the center of this spectral band of interest prompts consideration of its possible uses as an instrument for better understanding the interaction between NIR radiation and biomolecules such as cytochrome oxidase as well as its use as a diagnostic tool for assessing mitochondrial morphology and disease state.

Our work is distinguished from that in other laboratories which rely on light scattering techniques to study respiring mitochondria. Because the total and angular scattering intensity is a strongly oscillating function of organelle size, variations in size can lead to ambiguities in the scattering measurements. Our technique avoids this ambiguity in relative scattered light intensity by relying instead on absolute spectral intensity and spectral position. With further development, a biolaser developed for tiny organelles could rapidly determine the effects of neuroprotectants like cyclosporine A on mitochondria. This analysis could be very useful for rapid, front-end screen of pharmaceuticals. The entire testing process could be completed in minutes.

References

1. See for example, the recent issue of the journal devoted to this topic, M. Ferrari, editor, Journal of Biomedical Microdevices, Kluwer Academic Publishers, the Netherlands, vol 5, (2004).
2. Special Issue on Biomedical Applications for MEMS and Microfluidics, *Proceedings of the IEEE,* 92, No. 1, January 2004, A. Lee and R. B. Fair, *Guest Editors*
3. Microfabrication in biology and Medicine, J. Voldman, M. L. Gray, and M. A. Schmidt Annual Review of Biomedical Engineering, August 1999, Vol. 1, pp. 401-425
4. Handbook of Nanostructured Biomaterials and Their Applications in Nanobiotechnology, Edited by Hari Singh Nalwa American Scientific Publishers, Stevenson Ranch, California, 2004.
5. Microfluidic Memory and Control Devices, Alex Groisman,* Markus Enzelberger, Stephen R. Quake *Science* **300, 9** May 2003**,** pp 955-958.
6. Biocavity laser for high-speed cell and tumor biology, P. L. Gourley, , *J. Phys. D: Appl. Phys.* 36 No 14 (21 July 2003) R228-R239.
7. Biocavity Lasers**,** P. L.Gourley and D. Y. Sasaki, *American Scientist*, vol 89, April/May 2001, pp. 152-159.
8. Gourley, PL (1998), "NanoLasers," *Scientific American*, March issue, pp. 56-61.
9. Gourley, PL (1997) "Microlaser-Optical-Mechanical systems for biomedicine," *Optics and Photonics News*, April issue, pp. 31-36.
10. Gourley, PL, Meissner, KE, Brennan, TM, Hammons, BE (1995), "Surface-emitting Semiconductor Laser Spectroscopy for Characterizing Normal and Sickled Red Blood Cells," *Advances in Laser and Light Spectroscopy to Diagnose Cancer and Other Diseases II: Optical Biopsy*, SPIE 2387, pp.148-161.
11. Gourley, PL, McDonald, AE, Hendricks, JK, Copeland, GC, Hunter, J, Akhil, O, Dunne, JL, Skirboll, SL, Nihlen, L, and Capps, HJ, (2000), "Nanolaser/Microfluidic Biochip for Realtime Tumor Pathology," *J. Biomedical Microdevices,* 2, pp. 111-122.
12. Kessel, D, editor (1993) *Selected Papers on Photodynamic Therapy,* Society of Photo-Optical Instrumentation Engineers, (Bellingham, WA), 8194, pp 23-45.
13. Fujimoto, JG (1995) "Optical Biopsy an Imaging Using Optical Coherence Tomography," *Nature Medicine*, 1, pp. 970-972.
14. Block, SN, (1990) "Optical Trapping," *Noninvasive Techniques in Cell Biology,* Wiley-Liss New York, chap. 15.
15. Ashkin, A. and Dziedzic, JM, (1987), "Optical trapping of cells," *Science*. 235, pp. 1517-20.
16. Wiegand-Steubing, R (1991), *Cytometry* vol. 12, pp. 505-512.
17. Shapiro, HM (1988) *Practical Flow Cytometry*, 2nd Ed., Alan R. Liss, Inc. New York, book, chap. 1, pp. 115-198.
18. Gourley, PL, Akhil, O, Copeland, GC, Dunne, JL, Hendricks, JK, McDonald, AE, Skirboll, SL, Nihlen, L, (1999) "A semiconductor microlaser for intracavity flow cytometry," *Micro- and Nanofabricated Structures and Devices for Biomedical Applications*, SPIE 3606, pp. 64-73.
19. Alfano, RR and Katzir, A editors, (1996) "Advances in Laser and Light Spectroscopy to Diagnose Cancer and Other Diseases III: Optical Biopsy," SPIE 2679. pp 8-65.
20. Alfano, RR and Katzir, A editors, (1996) "Advances in Laser and Light Spectroscopy to Diagnose Cancer and Other Diseases III: Optical Biopsy," SPIE 2679. pp 2-7,66-93.
21. Nano-squeezed light for probing mitochondrial membrane swelling and study of neuroprotectants, P. L. Gourley, P. Chen, R. G. Copeland, J. D. Cox, J. K. Hendricks, A. E McDonald, D. Y. Sasaki, M. E. Keep and J. R. Karlsson, Proc. Conf on Microfluidics, BioMEMs, and Medical Microsystems, Photonics West, January 26-27, 2004, San Jose, CA, edited by P. Woias and I. Papautsky. p 51-60.
22. Nanolaser quickly analyzes neuroprotectant drugs, P. L. Gourley, Micro/Nano Newsletter, vol. 8 no. 1 Nov. 2003, p. 17, published by R&D Magazine.
23. Van de Hulst HC, *Light Scattering by Small Particles* (Dover Publications, New York, 1957).
24. Beavvoit B, T. Kitai, and B. Chance, "Contribution of the mitochondrial compartmentto the optical properties of a rat liver: a theoretical dna practical approach,: *Biophys. J.,* 67 2401-2410 (1994).
25. Brunsting A and Mullaney F, "Differential light scattering from spherical mammalian cells,: *Biophys. J.,* 14, 139-453 (1974).
26. Beuthan J, O. Milner, J. Hermann, M. Herrig, and G. Muller, *Phys. Med. Biol.,* 41 369 (1996).
27. Slot PMS, Hoekstra AG and Figdor CG, *Cytometry,* 9 636 (1988).

28. Mammer M, D. Schweitzer, B. Michel, E. Thamm, and A. Kolb, "Single scattering by red blood cells, *Appl. Opt.*, 37, 7410-7418 (1998).

29. Mourant JR, J. P. Freyer, A. H. Hielscher, A. A. Elick, D. Shen, and T. Johnson, "Mechanisms of light scattering from biological cells relevant to noninvasive optical-tissue diagnosis," *Appl. Opt.* 37, 3586-3593 (1998).

30. Hansson MJ, Persson T, Friberg H, Keep MF, Rees A, Wieloch T, Elmer E. Powerful cyclosporin inhibition of calcium-induced permeability transition in brain mitochondria. *Brain Res.* 960(1-2):99-111. Jan 17, 2003.

31. E. Carafoli and I. Roman, "Mitochondria and Disease," Molec. Aspects Med. 3 pp. 205-429, Pergamon Press Ltd. London, 1980.

32. M. F. Keep, K. S. K. Fong, K. Csiszar, and E. Elmer, "Cyclosporin A Prolongs Survival of SOD1 Mutant Mice and Implicates Mitochondrial Permeability Transition in Amyotrophic Lateral Sclerosis, *Immunosuppressant Analogs in Neuroprotection*, edited by C. V. Borlongan, O. Isacson, and P. R. Sanberg, Humana Press, Totowa, NJ, 2000, pp. 343-359.

33. M. F. Keep, H. Uchino, and E. Elmer, "Immunosuppressants as Neuroprotective Agents," *Immunosuppressant Analogs in Neuroprotection*, edited by C. V. Borlongan, O. Isacson, and P. R. Sanberg, Humana Press, Totowa, NJ, 2000, pp. 3-32.

34. S. Desagher and J-C. Martinou, "Mitochondria as the Central Control Point of Apoptosis," *Trends in Cell Biology*, 10 Sept. 2000, pp. 36 9-377.

35. T. E. Gunter, Karlene K. Gunter, S-S. Sheu, and C. E. Gavin, "Mitochondrial calcium transport: physiological and pathological relevance," *Am. J. Physiol.* 267, (1994), C313-C339.

36. A. B. Parekh, Store-operated Ca2+ entry: dynamic interplay between endoplasmic reticulum, mitochondria and plasma membrane, J. Physiol., 547(2), 2003, pp. 333 - 348.

37. D. D. Newmeyer and Ferguson-Miller, "Mitochondria: Releasing Power for Life and Unleashing the Machineries of Death," *Cell* 112 (2003) pp. 481-490.

38. S. Sola, M. A. Brito, D. Brites, J. J.G. Moura and C. M.P. Rodrigues, "Membrane structural changes support the involvement of mitochondria in the bile salt-induced apoptosis of rat hepatocytes," *Clinical Science* 103, (2002) pp. 475–485.

39. E. Jambrina, R. Alonso, M. Alcalde, M. Rodriguez, A. Serrano, C. Martinez-A., J. Garcia-Sancho, and M. Izquierdo, "Calcium influx through receptor-operated channel induces mitochondria-triggered paraptotic cell death," J. Bio. Chem. 278 pp. 14134-14145 (2003).

40. A. A. Fernando and J. F. Dice, "Protein translocation across membranes," Biochimica et Biophysica Acta 1513 (2001) pp. 1-24.

41. L He and J. J. Lemasters, "Heat shock suppresses the permeability transition in rat liver mitochondria," J. Bio. Chem. 278 (2003), pp. 16755-16760.

42. P. Bernardi, "the permeability transition pore: control points of a cyclosporine A-sensitive mitochondrial channel involved in cell death," Biochimica et Biophysica Acta 1275 (1996) pp. 5-9.

43. P. L. Pedersen, Tumor mitodhondria and the bioenergetics of cancer cells," *Prog. Exp. Tumor Res.* 22, pp. 190-274 (1978).

44. L. I. Grossman and E. A. Shoubridge, "Mitochondrial genetics and human disease," *BioEssays* 18 (12) (1996), pp. 983-991.

45. J. W. Shay and H. Werbin, "Are mitochondrial DNA mutations involved in the carcinogenic process?" *Mutation Research* 186 (1987) pp. 149-160.

46. Cooper, C.E., S. J. Matcher, J. S. Wyatt, M. Cope, G. C. Brown, E. M. Nemoto, and D. T. Delpy. Near-infrared spectroscopy of the brain: relevance to cytochrome oxidase bioenergetics. *Biochem. Soc. Trans.* 22: 974-980, 1994.

47. Ferrari, M., D. F. Hanley, D. A. Wilson, and R. T Traystman. Redox changes in cat brain cytochrome-c oxidase after blood-fluorocarbon exchange. *Am J Physiol Heart Circ Physiol*, 258: H1706 – 1713, 1990.

48. Hoshi, Y., H. Osamu, Y. Kakihana, and M. Tamura. Redox behavior of cytochrome oxidase in the rat brain measured by near-infrared spectroscopy. J Appl Physiol, 83: 1842 - 1848. 1997

Distribution

1			University of California, San Diego
			Attn: Robert K. Naviaux
			Departments of Medicine and Pediatrics
			San Diego, California, 92103-2071
1	MS	0123	Donna L. Chavez, 1011
10		1413	Paul Gourley, 1116
1		1413	Judy Hendricks, 1116
1		1413	Anthony McDonald, 1116
1		1415	Robert Copeland, 1112
1		9018	Central Technical Files, 8945-1
2		0899	Technical Library, 9616